

Commensurate structures in twisted transition metal dichalcogenide heterobilayers

Madeleine Phillips and C. Stephen Hellberg*
Naval Research Laboratory, Washington, D.C. 20375

(Dated: September 13, 2019)

A major theoretical challenge of studying twisted transition metal dichalcogenide (TMD) bilayers is that the unit cell of such structures is very large and therefore difficult to address using first-principles methods. However, twisted TMD bilayers form moiré patterns, which consist of regions of commensurate stacking, either smoothly interpolated into one another or separated by sharp domain walls. In this paper, we study twisted TMD bilayers by studying the properties of the constituent commensurate structures. Using density functional theory (DFT), we compute band structures for commensurately-stacked MoS_2/WS_2 and $\text{MoSe}_2/\text{WSe}_2$ bilayers in both 0° and 60° orientations, and we highlight variations in band structures across different commensurate geometries. These band structure variations arise from diverse factors such as metal atom asymmetry between layers (Mo vs. W), differences in interlayer hybridization, and Brillouin zone alignment. We comment on the consequences of such band structure differences for optical experiments and on the effects of strain on moiré pattern electronic structure.

In the advent of two-dimensional materials research, the most recent epoch has focused on stacks of 2D materials, known as van der Waals heterostructures^{1–3}. These heterostructures are characterized by strong bonds in the plane of each 2D layer and weak van der Waals bonds between layers. The weak interlayer coupling makes it possible to relax constraints related to lattice-matching and interlayer alignment and create stable heterostructures out of disparate materials in a wide variety of stacking orientations. Because heterostructure properties change when interchanging materials and altering interlayer geometry, this freedom opens the door for the creation of “designer materials,” whose properties can be tuned by careful choices of constituent layers and interlayer orientation.

One specific degree of freedom that has attracted much attention recently is the relative twist angle between layers. Famously, superconductivity emerges in bilayer graphene twisted at the “magic angle” of 1.05° ⁴, and topologically protected propagating states are pinned at the domain walls in bilayer graphene with small twist angles on the order of 0.25° ^{5,6}. In transition metal dichalcogenide (TMD) bilayers, the moiré pattern in off-commensurate samples, i.e. those twisted a small angle away from a commensurate stacking orientation, has been invoked to explain the photoluminescence signal of interlayer excitons^{7–9}.

A challenge of interpreting experiments carried out on small twist angle bilayers is that such systems have a very large repeat unit cell, making them prohibitively expensive to model using first-principles methods. This is in contrast to commensurately stacked bilayers, which can be described by a unit cell containing just twice as many atoms as the monolayer unit cell. One way to address this challenge becomes apparent when we note that the moiré patterns of small twist angle heterostructures contain distinct regions of commensurate stacking^{10–12}. Even better, Carr et al. have recently shown that homobilayers with sufficiently small twist angles should re-

construct into configurations dominated by commensurately stacked regions, which are separated only by narrow domain walls and nodes¹³. This reconstruction has been observed extensively in bilayer graphene^{14–16}, and we expect the same type of reconstruction to occur in both homo- and heterobilayer TMD structures. However, whether the transitions between commensurately stacked regions are smooth (as in the rigid moiré structure) or sharp (as in the reconstructed moiré), we can learn much about the electronic properties of twisted heterobilayers by studying the constituent commensurately stacked structures.

For monolayers with hexagonal lattices, such as 1H-TMD monolayers¹⁷, the commensurately stacked bilayer structures have layers oriented with a relative 0° or 60° twist (Figure 1). The geometries accessed by translating one layer of a 0° or 60° -oriented bilayer with respect to the other layer are also commensurate structures. Any of these stackings may appear in the corresponding off-commensurate twisted structures (e.g. $\theta = 1^\circ$ or $\theta = 59^\circ$ structures), and thus the study of the whole collection of 0° and 60° commensurate stackings is relevant for the study of small angle twisted bilayers¹⁰. In this paper, we study the configuration spaces of geometries associated with the 0° and 60° stacked TMD bilayers MoX_2/WX_2 , where $X=\text{S}$ or Se . Using first principles methods, we compute the electronic structures of the high-symmetry commensurate stackings. We focus on the high-symmetry geometries because these constitute the ground state and high energy structures in the energy landscapes of the 0° and 60° stacking spaces, and they are of special relevance in reconstructed moiré patterns^{13,18}. By examining the electronic structures of different commensurate geometries and comparing bilayer to monolayer band structures, we explore how band features are related to system symmetry, interlayer distance, and the difference in metal atoms between layers. Understanding the properties of commensurate geometries individually leaves us better equipped to predict the properties

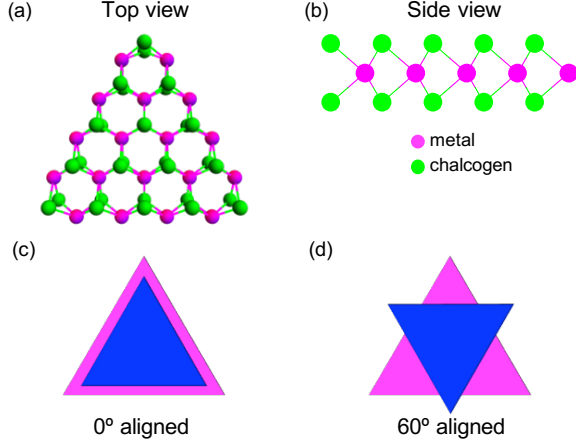


FIG. 1: (a) Schematic of a TMD monolayer in the 1H phase¹⁷. (b) Side view of a 1H TMD monolayer. Schematics of (c) 0° and (d) 60°-aligned TMD bilayers.

of twisted bilayers.

I. METHODS

First-principles calculations were carried out in a density functional theory (DFT) framework using the projector augmented wave (PAW) approach^{19,20} and the generalized gradient approximation (GGA)²¹ as implemented in VASP²². For the MoS₂/WS₂ bilayers, we use metal potentials with six valence electrons: $4d^55s^1$ for Mo and $5d^56s^1$ for W. For the S potential, the $n = 3$ electrons are included as valence electrons ($3s^23p^4$). For the MoSe₂/WSe₂ bilayers, the metal potentials we use have 14 valence electrons each: $4s^24p^64d^6$ for Mo and $5s^25p^65d^6$ for W, while the Se potential includes the $n = 4$ electrons as valence ($4s^24p^4$). In all cases we use at least an $8 \times 8 \times 1$ Γ -centered k-point mesh, a plane-wave energy cutoff of 450 eV, and an out of plane lattice constant of 30 Å, yielding a vacuum size of about 20 Å. We include the van der Waals interaction using the DFT-D3 method of Grimme²³.

II. RESULTS

We carried out first-principles calculations for four distinct systems: MoS₂/WS₂ and MoSe₂/WSe₂ bilayers in the 0° and 60° stacking orientations. The geometry of each system is further specified by $\mathbf{r}(\alpha, \beta)$, which describes the lateral shift of the top layer relative to the bottom layer while keeping the angular orientation fixed. We study translations of the top layer described by the following expression:

$$\mathbf{r}(\alpha, \beta) = \alpha \mathbf{r}_1 + \beta \mathbf{r}_2, \quad (1)$$

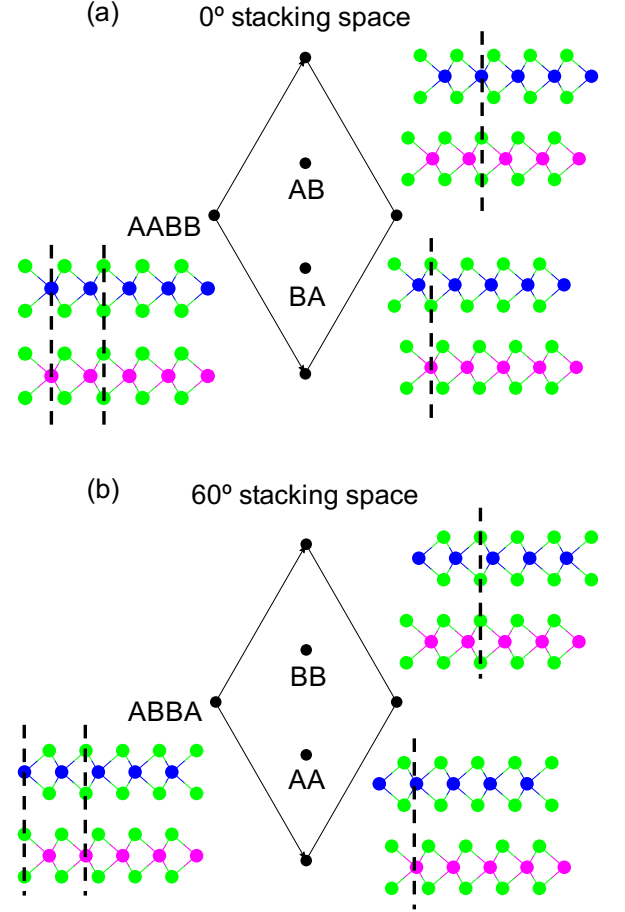


FIG. 2: Stacking spaces of (a) 0°- and (b) 60°-aligned TMD bilayers, with high-symmetry stackings labelled and depicted in side view. High-symmetry stackings are specified by a two or four letter label, where A refers to metal sites, and B refers to chalcogen sites. The first and third letter in a label refer to sites in the top layer, and the 2nd and 4th letter in a label refer to sites in the bottom layer. E.g. The label AABB refers to a stacking geometry where top layer metals are aligned over bottom layer metals, and top layer chalcogens are aligned over bottom layer chalcogens (A site over A site and B site over B site).

where $\mathbf{r}_1 = a(\frac{\sqrt{3}}{2}, -\frac{1}{2})$ and $\mathbf{r}_2 = a(\frac{\sqrt{3}}{2}, \frac{1}{2})$ are the in-plane lattice vectors, a is the lattice constant, and α, β are numbers between 0 and 1. The stacking geometries induced by various interlayer translations \mathbf{r} can be plotted on a real-space unit cell for each angular orientation (Figure 2). High symmetry stacking geometries are labelled by pairs or quadruplets of letters. In our labelling convention, ‘A’ refers to a metal atom and ‘B’ to a chalcogen atom. A pair of letters in the stacking designation indicates sites aligned in the top and bottom layers, respectively. For example “AA” refers to a stacking geometry where metals in the top layer are aligned with metals in the bottom layer (A site over A site), and “ABBA” refers to a geometry where a top layer metal is aligned with bottom layer chalcogens and top layer chalcogens are aligned

over a bottom layer metal (A site over B site and B site over A site). Stacking designations with four letters have two pairs of sites aligned in the top and bottom layers, while stacking designations with two letters have only one pair of aligned sites. The stacking geometry that corresponds to no interlayer translation $\mathbf{r}(0,0)$ is AABB for the 0° -oriented bilayer and ABBA for a 60° -oriented bilayer. These geometries appear on all four corners of their respective 0° or 60° stacking spaces (Figure 2).

We computed the vacuum-aligned band structures of the high symmetry stacking geometries in the 0° and 60° -oriented MoS_2/WS_2 and $\text{MoSe}_2/\text{WSe}_2$ bilayers, since these are the extrema in stacking energy landscapes. For the sulfide and selenide heterobilayers we study, the ground state stacking for the 60° -aligned bilayers is ABBA, and the 0° -aligned bilayers have two degenerate stacking geometries: AB and BA. The highest energy stacking is AABB for the 0° -aligned bilayers and BB for the 60° -aligned bilayers. In the 60° -aligned sulfide bilayer, AA stacking is a local minimum in energy¹⁸.

In the following, we focus on the ground state stacking geometries for two reasons. First, ground state stackings are expected to dominate the reconstructed moiré patterns of small angle twisted bilayers¹³. Second, the minimum band gap in each configuration space occurs in a low-energy structure, and we expect excitons in moiré bilayers to drift towards the region of minimum gap. Band structures for non-ground state high symmetry stackings are shown in the Supplemental Material²⁴. All structures were relaxed with the metal atoms fixed in the x-y plane and allowed to relax in the z-direction (along the layer normal). Chalcogens were allowed to relax in all three cartesian directions. The lattice constants used in each system were $a(\text{S}, 0^\circ)=3.167 \text{ \AA}$, $a(\text{S}, 60^\circ)=3.166 \text{ \AA}$, $a(\text{Se}, 0^\circ)=3.295 \text{ \AA}$, and $a(\text{Se}, 60^\circ)=3.293 \text{ \AA}$, where each value was computed by minimizing energy with respect to lattice constant in the BA structure for 0° degree oriented bilayers and in the ABBA structure for 60° degree oriented bilayers. The difference between optimized lattice constants for the high symmetry geometries is less than 0.1% in every case, so we judge that it is reasonable to use the same lattice constant for each geometry in a given stacking space.

We computed band structures that include the effects of spin-orbit interactions. Inversion symmetry is broken in heterobilayers, and the presence of the heavy element tungsten makes the spin-orbit splittings significant. Because we use GGA functionals in our DFT calculations, the band gaps we report are significantly smaller than expected experimental values. However, energy differences are expected to be more reliable, and we focus on these in the results that follow^{25,26}.

Figure 3 shows vacuum-aligned band structures of the ground state stacking geometries of $\text{MoSe}_2/\text{WSe}_2$ and MoS_2/WS_2 bilayers, with the band gap size labeled for all band structures and the Q-point spin-orbit splitting labeled on the selenide band structures. All of the ground state structures have Type II band alignment at the K

point, with the states at the valence band edge localized in the WX_2 layer and the states at the conduction band edge localized in the MoX_2 layer. The four lowest conduction bands at K are layer-polarized, i.e. there is no hybridization between layers. In the valence band, the band edge corresponds to states well-localized in the WX_2 layer, but the second through fourth valence bands have different interlayer hybridizations depending on the structure. Most notable are the differences in hybridization between the ground state structures in the 0° vs. 60° -oriented bilayers. The third and fourth valence bands in the AB and BA structures are well layer-polarized, even though bands of the same spin are quite close in energy, whereas there is significant mixing between layers in the second and third valence bands in the ABBA structure (Figure 4).

The minimum gap in the $\text{MoSe}_2/\text{WSe}_2$ ground states is indirect from the K to the Q point, where Q is a point lying between K and Γ . While the indirect nature of the selenide bilayer band gap does depend on strain (Figure 5), literature values for the thermal expansion coefficient²⁷ suggest that temperature effects are not enough to induce a direct gap at the sub-100K temperature scales in recent experiments^{7,9}. The band gaps for the ground state structures are still squarely in the indirect gap regime at temperatures near 100K, while the AA and BB structures in the 60° -aligned bilayer are very close to being direct gap. In our 0K calculations, both the gap size and the magnitude of the spin-orbit splitting at the Q point differ among the three ground state structures, as shown in Figure 3 (a)-(c). Even the degenerate 0° stackings AB and BA have band gaps that differ by 78 meV and Q point splittings that differ by 24 meV, which are energy scales accessible in optical experiments.

In the ground state stacking geometries of the MoS_2/WS_2 bilayer, the band gap is indirect, with the valence band maximum at the Γ point and the conduction band minimum at the K point. As in the selenides, the band gap varies across geometries, but curiously, the 60° -aligned ground state (ABBA) and one of the 0° -aligned ground states (AB) have band gaps of the same size, while the other 0° -aligned ground state (BA) has a band gap 58 meV smaller than its partner.

III. DISCUSSION

We study exclusively commensurate stackings of TMD heterobilayers in this work, so in some ways the structures we consider are all very similar. However, the results reported above highlight a wide variety of both similarities and differences between the electronic structures of the various geometries. For instance, we find that the two energetically degenerate ground states in the 0° stacking space have very different band gaps. This is true whether the chalcogens in the bilayer are sulfurs or seleniums, implying that there is an important generic difference between the AB and BA structures. In the

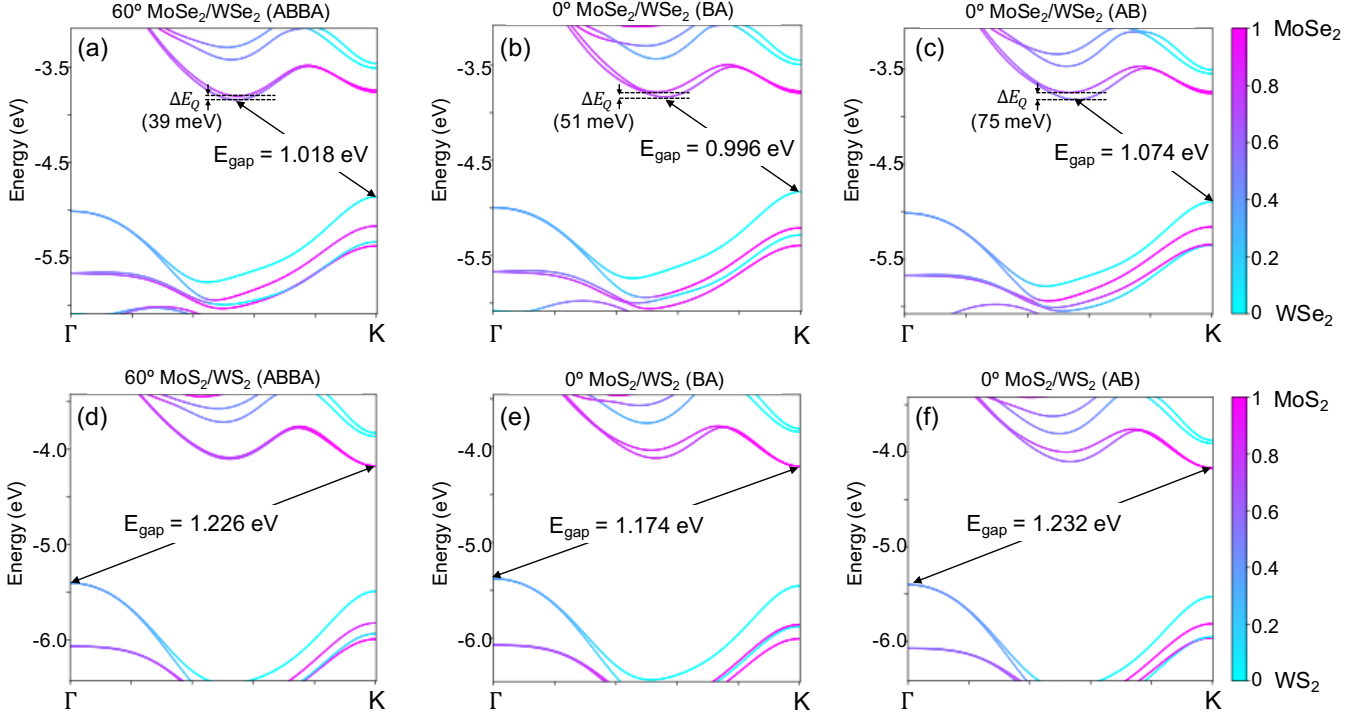


FIG. 3: Vacuum-aligned band structures of the ground state stacking geometries in (a) 60°-aligned MoSe₂/WSe₂ and (b), (c) 0°-aligned MoSe₂/WSe₂, as well as (d) 60°-aligned MoS₂/WS₂ and (e), (f) 0°-aligned MoS₂/WS₂. Bands are plotted from Γ to K. The color scale indicates the layer weight of each state, with cyan corresponding to all weight coming from the WX₂ layer and magenta corresponding to all weight coming from the MoX₂ layer (X=S, Se). The selenide bilayers exhibit an indirect gap from K to Q, while the sulfide bilayers have an indirect gap from Γ to K. The degenerate ground state stacking geometries in the 0°-oriented systems (BA and AB) have distinct band gaps and conduction band Q-point splittings. The vacuum-alignment of the band structures allows us to compare absolute band edge positions between different geometries within a given material.

discussion that follows, we identify some chemical and symmetry-related factors that contribute to the similarities and differences between various structures and materials.

To understand the differences in band structure across distinct stacking geometries, it's instructive to compare bilayer bands to the constituent monolayer bands. In homobilayer calculations, the bilayer and monolayer band structures would be identical in the absence of interlayer coupling. Indeed, for homobilayers the offset between bilayer bands corresponding to different layers is a direct proxy for the strength of interlayer coupling¹⁰. One of the challenges of interpreting heterobilayer band structures is distinguishing bilayer band structure features that arise from interlayer coupling from those that arise from the “hetero-” nature of the bilayer (i.e. the different metal atoms in the two layers). In the top half of each panel in Figure 4, we show the valence bands of aligned monolayers, where we have aligned the MoX₂ and WX₂ bands by matching the monolayer conduction band edges to the pure state conduction bands at K in various bilayer geometries. (See Supplemental Material for full aligned monolayer band structures²⁴.) In this way, we can compare the band offsets that arise from the difference in

metal atoms without any interlayer coupling effects. The bottom half of each panel in Figure 4 shows the valence bands of the fully interacting bilayer with the hybridizations at the K point labelled. We use these hybridizations as a proxy for interlayer coupling strength. Some combination of interlayer coupling, the difference in metal atoms, and symmetry considerations contributes to variations in band structure across stacking geometries, and we comment on these factors below.

The effect of the metal asymmetry on band gap size in our heterobilayers is most apparent when comparing the AB and BA structures in the MoSe₂/WSe₂ bilayer. The band gap in both structures is from the K point in the valence band to the Q point in the conduction band, and the overall difference in band gap between the two structures is 78 meV. The difference in Q point minimum in AB vs. BA is only 9 meV, so most of the band gap difference arises from the difference in the valence band maxima (VBM) at K. The difference in VBM cannot be a function of differences in interlayer metal-to-metal distance since this is roughly the same in the AB and BA structures (see Figure S6²⁴), and it can't be a consequence of hybridization pushing bands apart since there is little to no hybridization at the top of the va-

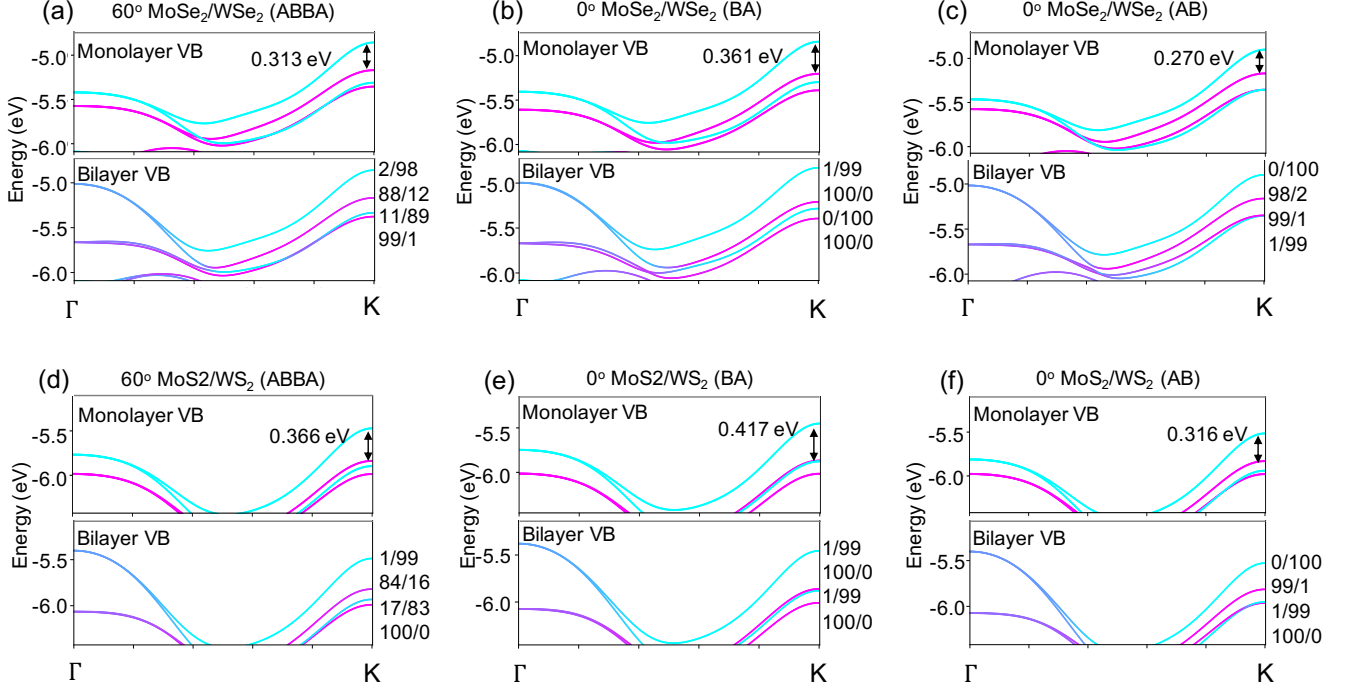


FIG. 4: Valence bands for monolayers and bilayers in the low energy structures. The top half of each panel shows the monolayer valence bands, which have been aligned to the corresponding bilayer band structure. The bottom half of each panel shows the bilayer valence bands. The color scale is the same as that in Figure 3, with the magenta bands corresponding to states localized on the MoX_2 layer and the cyan bands corresponding to states localized on the WX_2 layer. The monolayer bands are aligned to the corresponding bilayer structure by matching the conduction band edge at K in MoX_2 to the conduction band edge at K in the bilayer and the conduction band edge at K in WX_2 to the second band above the conduction band edge in the bilayer, since the lowest four conduction bands in each bilayer at K are “pure” states with no interlayer hybridization (See Figure 3.) The bottom half of each panel shows the degree of valence band hybridization at K in each geometry. The pairs of numbers X/Y indicate that for a given band, the corresponding state at K has X% of its weight on the MoX_2 layer and Y% of its weight in the WX_2 layer.

lence band at K in these structures (bottom sections of Figure 4 (b), (c)). We instead conjecture that the difference in band edge alignment between monolayer bands in AB as compared to BA is a consequence of the different dielectric environments of the metal atoms, since metal atom orbitals dominate the monolayer band edges at K²⁸. In the AB structure, the W atoms are surrounded by a greater number of chalcogens, whereas in the BA structure, the Mo atoms are surrounded by the greater number of chalcogens. We can estimate the size of this effect by measuring the monolayer band offsets at the VBM in the aligned monolayers in Figure 4. The difference in monolayer band offsets is about 91 meV between the AB and BA structures, with the band offset higher in BA, which has the smaller bilayer band gap. The argument that these band offsets come from the metal atom asymmetry in our bilayers is strengthened by the fact that the difference between monolayer band offsets at K in the AB and BA structures of the MoS_2/WS_2 is roughly the same (within 10 meV) as the selenide bilayer, despite the difference in chalcogen.

Interlayer hybridization can also explain some of the

variation in band structures across geometries. For instance, in the selenide bilayers it is the hybridization of bands at the Q point that pushes the Q-point conduction bands below the bands at K, making the selenide heterobilayers indirect gap materials in contrast to the direct gap monolayer MoSe_2 . In the sulfide bilayers, it is the hybridization of the valence bands at Γ that gives the bilayers their indirect gap, as seen by comparing the aligned monolayer and bilayer valence bands in Figure 4. (The exception is the high energy BB and AABBS sulfide structures, where hybridization at Γ is not strong enough to shift the Γ point higher than the K point, probably due to the large interlayer distance in the high energy stackings. See Figures S1 and S2²⁴.)

Interlayer hybridization and the splitting of bands that results is a function of interlayer distance and the energy offset of the unhybridized bands¹². However, the alignment of a system can also effect the mixing, a fact exemplified by the differences in hybridization near the valence band edge at K in ABBA vs. AB and BA structures. The orbitals at the valence band edges are predominantly metal d orbitals, and for the specific metal atom

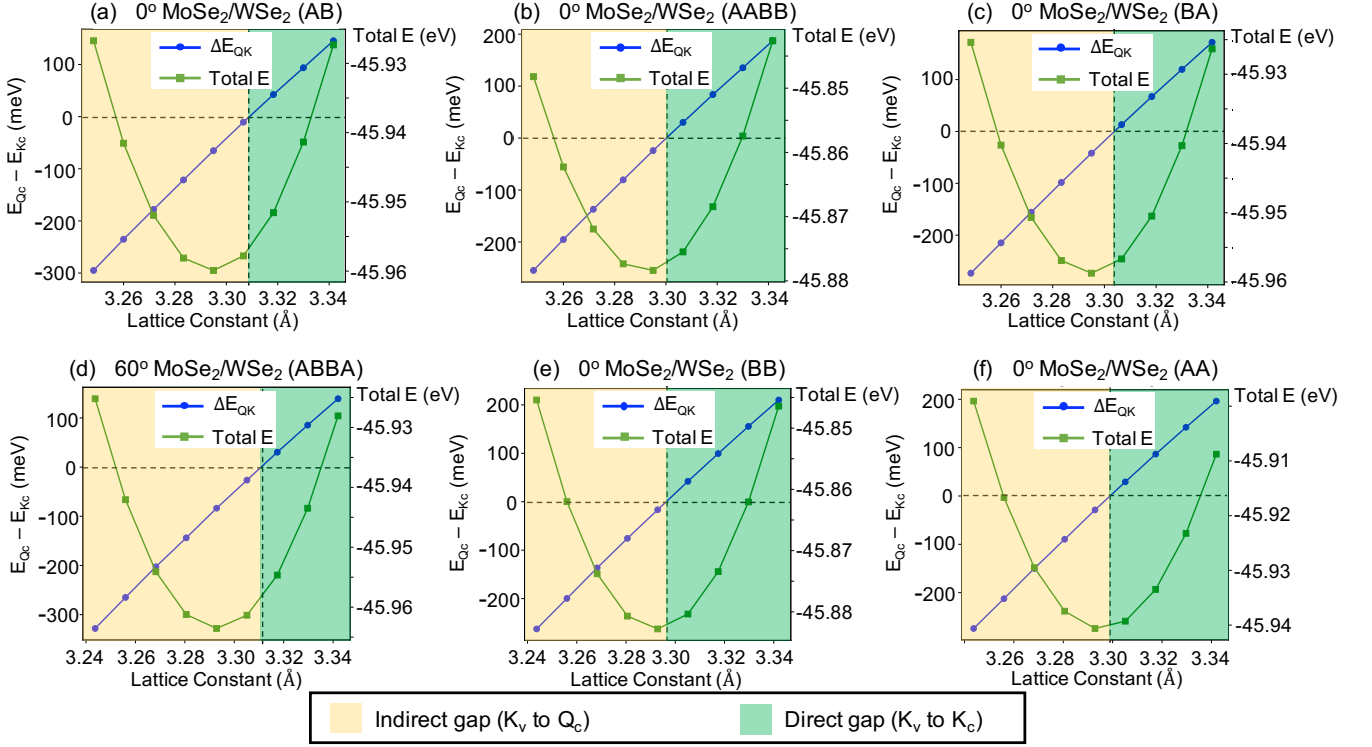


FIG. 5: The indirect or direct nature of the band gap in the selenides depends sensitively on the choice of lattice constant. Here we plot the energy difference between conduction band minima at the K point and the Q point (blue curve) and the total energy (green curve) against lattice constant for the high symmetry stackings of 0° and 60°-aligned MoSe₂/WSe₂ bilayers. The optimized lattice constant for each structure is the value at the minimum of the total energy parabola. The parabolic shape of the energy curve shows that we are straining the bilayers in the elastic regime. Lattice constants for which a structure has an indirect gap from K in the valence band to Q in the conduction band are highlighted in yellow, while lattice constants for which a structure has a direct gap at K are highlighted in green. Each structure has an indirect gap at the optimized lattice constant, and the gap becomes direct for tensile biaxial strain greater than (a) 0.46% (b) 0.24% and (c) 0.30% for the 0° AB, AAB, and BA structures and (d) 0.55% (e) 0.12% and (f) 0.12% for the 60° ABBA, BB, and AA structures, respectively.

symmetry of the ABBA structure, there should be finite mixing between Mo and W bands at the valence band edge at K²⁸. Indeed we find finite hybridization between the valence bands with the same spin at K in both the sulfide and selenide bilayers (Figure 4 (a), (d)). The AB and BA structures have the same metal atom symmetry as ABBA, so we would naively expect to find finite mixing in the valence band at K in both structures. However sulfide and selenide AB and BA heterobilayers all show negligible interlayer mixing between valence bands with the same spin at K (Figure 4 (b)-(c), (e)-(f)). This discrepancy arises from the distinct Brillouin zone alignments in 0° vs. 60° structures. In the 0°-aligned AB and BA structures, the K points are aligned, while in the 60°-aligned ABBA structure, the K point in one layer is aligned with the K' point in the other layer. Since the K and K' points are time-reversed partners, the wavefunctions at these points are related by complex conjugation. This difference in the phase of the wavefunctions at K and K' causes the contribution to the interlayer hopping term to cancel out in the 0°-aligned structure, forbidding hybridization at the level of the metal-atom tight-binding

model.

The differences in band gap size and location as well as spin-orbit splitting in the various stacking geometries should have consequences for photoluminescence (PL) of the heterobilayers. Hanbicki, et al. argue²⁹ that the splitting of the interlayer exciton (ILE) peak in PL measurements corresponds to the spin-orbit splitting at the Q point of the bilayer electronic structure. If this is the case, then different geometries could be distinguished by ILE peak splitting as well as by ILE peak location. For example, the PL signal for a MoSe₂/WSe₂ bilayer in the AB stacking geometry would have an ILE peak at an energy about 78 meV higher than a bilayer in the BA stacking geometry, and the peak splitting would be 24 meV larger for the AB stacked bilayer. Furthermore, the strain-dependence of the band gaps could have an effect on optical experiments, particularly in moiré bilayers, where strain effects can be significant. Under sufficient tensile strain, selenide heterobilayers will become direct gap, which might quench the ILE signal altogether, since the wavefunctions at the valence band maximum and conduction band minimum at K are in separate lay-

ers and thus have no overlap.

IV. CONCLUSION

One route to understanding experiments on twisted TMD heterostructures is to understand the properties of the constituent commensurate regions of such moiré structures. In this paper, we used first-principles calculations to compute electronic structure of commensurately stacked $\text{MoSe}_2/\text{WSe}_2$ and MoS_2/WS_2 bilayers in both the 0° and 60° orientations. We identify variations in band gap and spin-orbit splitting, which arise from the metal atom asymmetry of the heterobilayers and differences in interlayer hybridization. These results may allow the stacking structure of heterobilayers to be probed

using optical techniques.

Acknowledgements

We acknowledge H.-J. Chuang, A. T. Hanbicki, B. T. Jonker, I. I. Mazin, K. M. McCreary, M. R. Rosenberger, S. V. Sivaram, and D. Wickramaratne for helpful discussions. This research was performed while M.P. held a National Research Council fellowship at NRL. This work was supported by core programs at NRL and the NRL Nanoscience Institute. Computational work was supported by a grant of computer time from the DoD High Performance Computing Modernization Program at the U.S. Army Research Laboratory and the U.S. Air Force Research Laboratory Supercomputing Resource Centers.

-
- * Electronic address: steve.hellberg@nrl.navy.mil
- ¹ T. Niu and A. Li, “From two-dimensional materials to heterostructures,” *Progress in Surface Science*, vol. 90, no. 1, pp. 21–45, 2015.
 - ² A. K. Geim and I. V. Grigorieva, “Van der Waals heterostructures,” *Nature*, vol. 499, no. 7459, pp. 419–425, 2013.
 - ³ Y. Liu, N. O. Weiss, X. Duan, H.-C. Cheng, Y. Huang, and X. Duan, “Van der waals heterostructures and devices,” *Nature Reviews Materials*, vol. 1, pp. 16042 EP –, Jul 2016. Review Article.
 - ⁴ Y. Cao, V. Fatemi, S. Fang, K. Watanabe, T. Taniguchi, E. Kaxiras, and P. Jarillo-Herrero, “Unconventional superconductivity in magic-angle graphene superlattices,” *Nature*, vol. 556, pp. 43–50, Apr. 2018.
 - ⁵ F. Zhang, A. H. MacDonald, and E. J. Mele, “Valley Chern numbers and boundary modes in gapped bilayer graphene,” *Proceedings of the National Academy of Sciences*, vol. 110, pp. 10546–10551, June 2013.
 - ⁶ S. Huang, K. Kim, D. K. Efimkin, T. Lovorn, T. Taniguchi, K. Watanabe, A. H. MacDonald, E. Tutuc, and B. J. LeRoy, “Topologically Protected Helical States in Minimally Twisted Bilayer Graphene,” *Physical Review Letters*, vol. 121, p. 037702, July 2018.
 - ⁷ K. Tran, G. Moody, F. Wu, X. Lu, J. Choi, K. Kim, A. Rai, D. A. Sanchez, J. Quan, A. Singh, J. Embley, A. Zepeda, M. Campbell, T. Autry, T. Taniguchi, K. Watanabe, N. Lu, S. K. Banerjee, K. L. Silverman, S. Kim, E. Tutuc, L. Yang, A. H. MacDonald, and X. Li, “Evidence for moiré excitons in van der Waals heterostructures,” *Nature*, vol. 19, pp. 1–13, Feb. 2019.
 - ⁸ C. Jin, E. C. Regan, A. Yan, M. I. B. Utama, D. Wang, S. Zhao, Y. Qin, S. Yang, Z. Zheng, S. Shi, K. Watanabe, T. Taniguchi, S. Tongay, A. Zettl, and F. Wang, “Observation of moiré excitons in WSe_2/WS_2 heterostructure superlattices,” *Nature*, vol. 567, pp. 76–80, Mar. 2019.
 - ⁹ K. L. Seyler, P. Rivera, H. Yu, N. P. Wilson, E. L. Ray, D. G. Mandrus, J. Yan, W. Yao, and X. Xu, “Signatures of moiré-trapped valley excitons in $\text{MoSe}_2/\text{WSe}_2$ heterobilayers,” *Nature*, pp. 1–17, Feb. 2019.
 - ¹⁰ Y. Wang, Z. Wang, W. Yao, G.-B. Liu, and H. Yu, “Interlayer coupling in commensurate and incommensurate bilayer structures of transition-metal dichalcogenides,” *Physical Review B*, vol. 95, no. 11, p. 115429, 2017.
 - ¹¹ Q. Tong, H. Yu, Q. Zhu, Y. Wang, X. Xu, and W. Yao, “Topological mosaics in moiré superlattices of van der waals heterobilayers,” *Nature Physics*, vol. 13, pp. 356 – 362, Nov 2016.
 - ¹² P. Rivera, H. Yu, K. L. Seyler, N. P. Wilson, W. Yao, and X. Xu, “Interlayer valley excitons in heterobilayers of transition metal dichalcogenides,” *Nature Nanotechnology*, vol. 10, p. 1, Aug. 2018.
 - ¹³ S. Carr, D. Massatt, S. B. Torrisi, P. Cazeaux, M. Luskin, and E. Kaxiras, “Relaxation and domain formation in incommensurate two-dimensional heterostructures,” *Physical Review B*, vol. 98, no. 22, p. 224102, 2018.
 - ¹⁴ J. S. Alden, A. W. Tsen, P. Y. Huang, R. Hovden, L. Brown, J. Park, D. A. Muller, and P. L. McEuen, “Strain solitons and topological defects in bilayer graphene,” *Proceedings of the National Academy of Sciences*, vol. 110, pp. 11256–11260, July 2013.
 - ¹⁵ S. S. Sunku, G. X. Ni, B. Y. Jiang, H. Yoo, A. Sternbach, A. S. McLeod, T. Stauber, L. Xiong, T. Taniguchi, K. Watanabe, P. Kim, M. M. Fogler, and D. N. Basov, “Photonic crystals for nano-light in moiré graphene superlattices,” *Science*, vol. 362, pp. 1153–1156, Dec. 2018.
 - ¹⁶ H. Yoo, R. Engelke, S. Carr, S. Fang, K. Zhang, P. Cazeaux, S. H. Sung, R. Hovden, A. W. Tsen, T. Taniguchi, K. Watanabe, G.-C. Yi, M. Kim, M. Luskin, E. B. Tadmor, E. Kaxiras, and P. Kim, “Atomic and electronic reconstruction at the van der Waals interface in twisted bilayer graphene,” *Nature Materials*, vol. 18, pp. 448–453, May 2019.
 - ¹⁷ Giving a monolayer the “H” label is something of an abuse of notation, since H usually refers to the 60° stacking between multiple monolayers, as in bilayer 2H TMDs. Here we use the H designation to indicate that the relative positions of metal and chalcogens within a monolayer is the same as that found in the monolayer components of 2H TMDs. This distinguishes our monolayers from 1T or 1T’ monolayers, where the chalcogen atoms are displaced from the positions they occupy with respect to the metal atoms in 2H phase (or indeed 3R and bulk) TMDs.
 - ¹⁸ Rosenberger et al., in preparation.

- ¹⁹ P. E. Blöchl, “Projector augmented-wave method,” *Physical Review B*, vol. 50, no. 24, pp. 17953–17979, 1994.
- ²⁰ G. Kresse and D. Joubert, “From ultrasoft pseudopotentials to the projector augmented-wave method,” *Physical Review B*, vol. 59, no. 3, pp. 1758–1775, 1999.
- ²¹ J. P. Perdew, K. Burke, and M. Ernzerhof, “Generalized Gradient Approximation Made Simple,” *Physical Review Letters*, vol. 77, no. 18, pp. 3865–3868, 1996.
- ²² G. Kresse and J. Furthmüller, “Efficient iterative schemes for *ab initio* total-energy calculations using a plane-wave basis set,” *Physical Review B*, vol. 54, no. 16, pp. 11169–11186, 1996.
- ²³ S. Grimme, J. Antony, S. Ehrlich, and H. Krieg, “A consistent and accurate *ab initio* parametrization of density functional dispersion correction (DFT-D) for the 94 elements H–Pu,” *The Journal of Chemical Physics*, vol. 132, no. 15, p. 154104, 2010.
- ²⁴ See Supplemental Material at [URL] for additional band structure plots.
- ²⁵ A. Kormányos, G. Burkard, M. Gmitra, J. Fabian, V. Zólyomi, N. D. Drummond, and V. Fal’ko, “k-p theory for two-dimensional transition metal dichalcogenide semiconductors,” *2D Materials*, vol. 2, p. 022001, June 2015.
- ²⁶ J. Kang, S. Tongay, J. Zhou, J. Li, and J. Wu, “Band offsets and heterostructures of two-dimensional semiconductors,” *Applied Physics Letters*, vol. 102, no. 1, p. 012111, 2013.
- ²⁷ C. Sevik, “Assessment on lattice thermal properties of two-dimensional honeycomb structures: Graphene, h-BN, h-MoS₂, and h-MoSe₂,” *Physical Review B*, vol. 89, p. 035422, Jan. 2014.
- ²⁸ A. M. Jones, H. Yu, J. S. Ross, P. Klement, N. J. Ghimire, J. Yan, D. G. Mandrus, W. Yao, and X. Xu, “Spin-layer locking effects in optical orientation of exciton spin in bilayer WSe₂,” *Nature Physics*, vol. 10, pp. 130–134, Feb. 2014.
- ²⁹ A. T. Hanbicki, H.-J. Chuang, M. R. Rosenberger, C. S. Hellberg, S. V. Sivaram, K. M. McCreary, I. I. Mazin, and B. T. Jonker, “Double Indirect Interlayer Exciton in a MoSe₂/WSe₂ van der Waals Heterostructure,” *ACS Nano*, vol. 12, no. 5, pp. 4719–4726, 2018.

Supplement to Commensurate structures in twisted transition metal dichalcogenide heterobilayers

Madeleine Phillips and C. Stephen Hellberg
Naval Research Laboratory, Washington, D.C. 20375

¹ S. Carr, D. Massatt, S. B. Torrisi, P. Cazeaux, M. Luskin, and E. Kaxiras, "Relaxation and domain formation in incommensurate two-dimensional heterostructures," *Physical Review B*, vol. 98, no. 22, p. 224102, 2018.

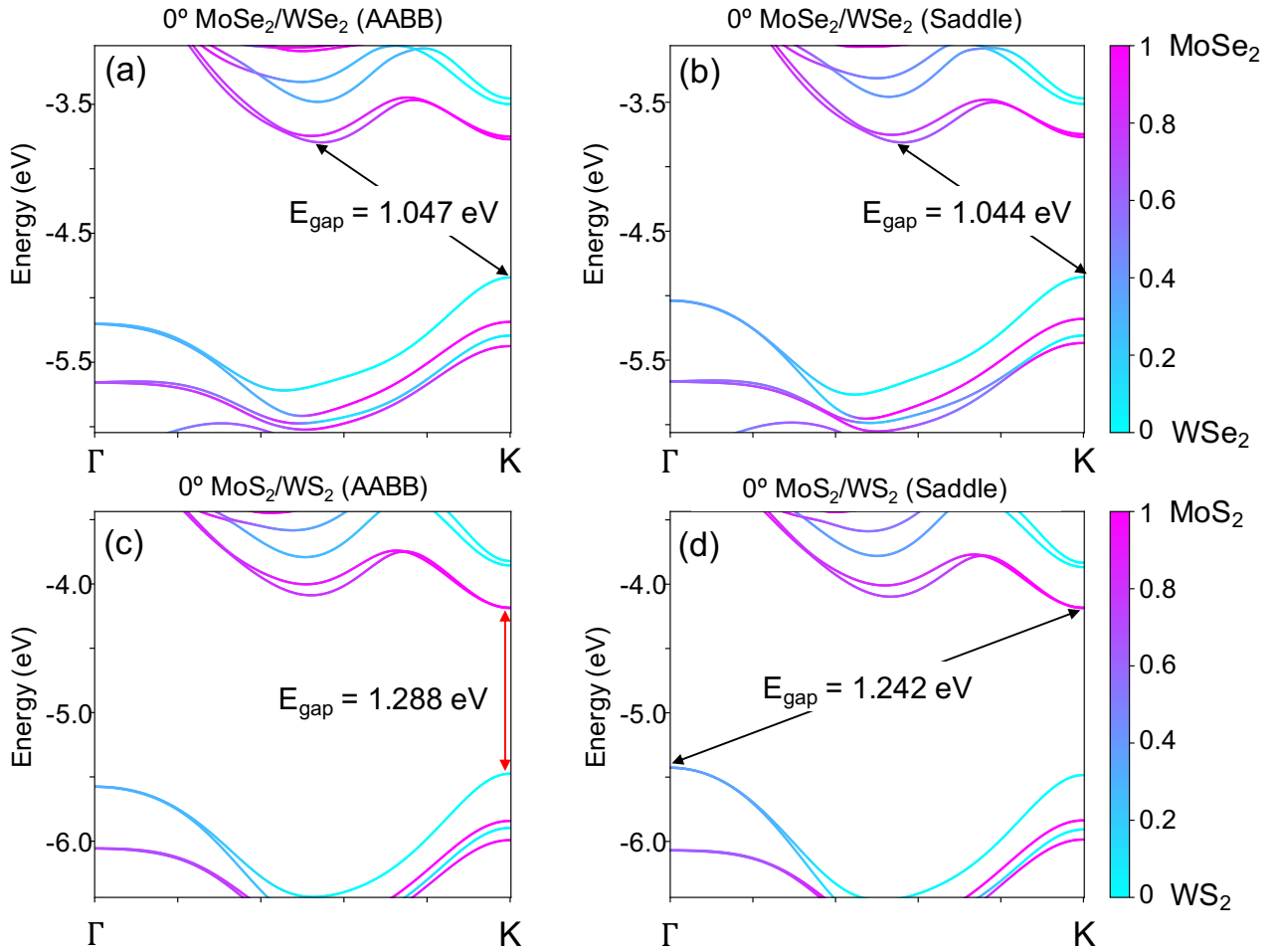


FIG. S1: Remaining high symmetry band structures for 0°-aligned (a)-(b) MoSe₂/WSe₂ and (c)-(d) MoS₂/WS₂ bilayers. AABB is the high energy structure at $(\alpha, \beta) = (0, 0)$ and the Saddle point structure is halfway between the AB and BA structures at $(\alpha, \beta) = (1/2, 1/2)$. The band structures in both materials have a type II band alignment at K. As in the other selenide bilayer structures, the AABB and Saddle point stackings have an indirect gap from K in the valence band to Q in the conduction band. The saddle point structure in the sulfide bilayer has an indirect gap from Γ in the valence band to K in the conduction band, like the other sulfide band structures. However, the high energy AABB sulfide bilayer has a direct gap at K, with a magnitude larger than any other 0°-aligned sulfide bilayer band gap in this study.

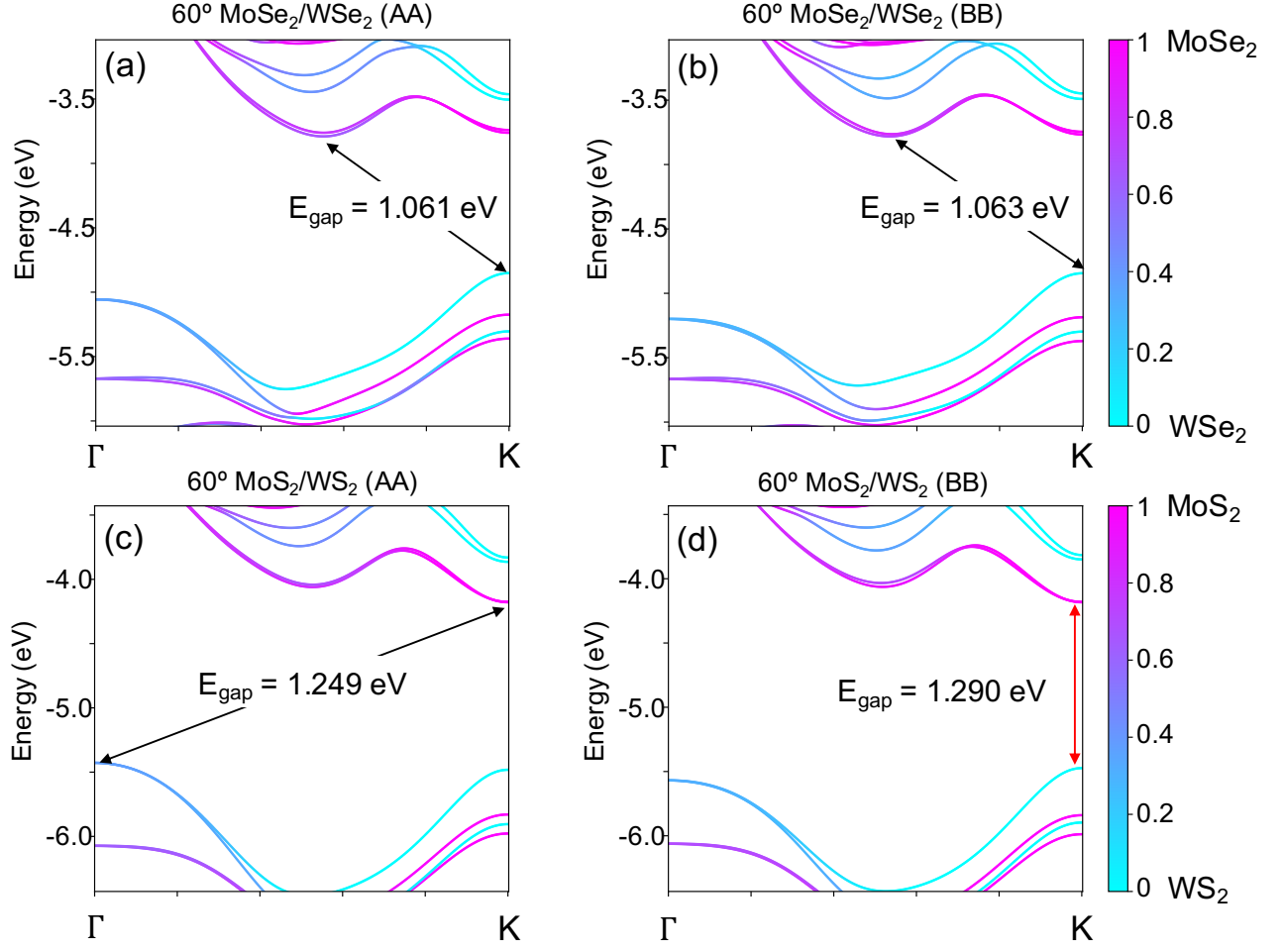


FIG. S2: Remaining high symmetry band structures for 60°-aligned (a)-(b) MoSe₂/WSe₂ and (c)-(d) MoS₂/WS₂ bilayers. AA is a structure located at $(\alpha, \beta) = (2/3, 1/3)$ in the 60° configuration space. In the sulfide bilayer, AA is a local minimum, and indeed some calculations of sulfide homobilayers like MoS₂/MoS₂ find the AA structure to be the global minimum¹. The BB structure is the high energy structure in the 60° configuration space, located at $(\alpha, \beta) = (1/3, 2/3)$. The band structures in both materials have a type II band alignment at K. As in the other selenide bilayer structures, the AA and BB stackings have an indirect gap from K in the valence band to Q in the conduction band. The AA structure in the sulfide bilayer has an indirect gap from Γ in the valence band to K in the conduction band, like the other sulfide band structures. However, the high energy BB sulfide bilayer has a direct gap at K, with a magnitude larger than any other 60°-aligned sulfide bilayer band gap in this study.

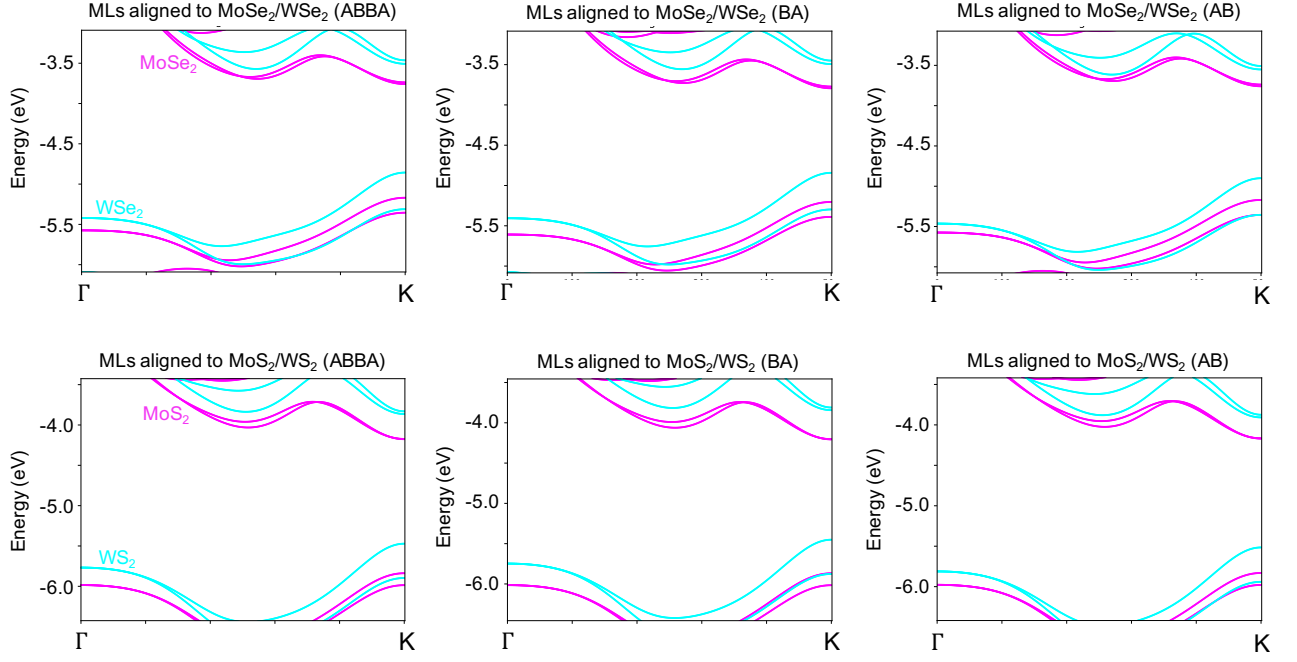


FIG. S3: Aligned monolayer bands for ground state structures in 0° and 60° stacking spaces. The conduction band edge of each monolayer at K is aligned with the appropriate bilayer pure state at K. (i.e. The MoX₂ conduction band edge is aligned with the bilayer conduction band minimum, which is entirely localized in the MoX₂ layer, and the WX₂ conduction band edge is aligned with the third lowest bilayer conduction band at K, which is entirely localized on the WX₂ layer.) Magenta bands are the MoX₂ bands and cyan bands are the WX₂ bands.

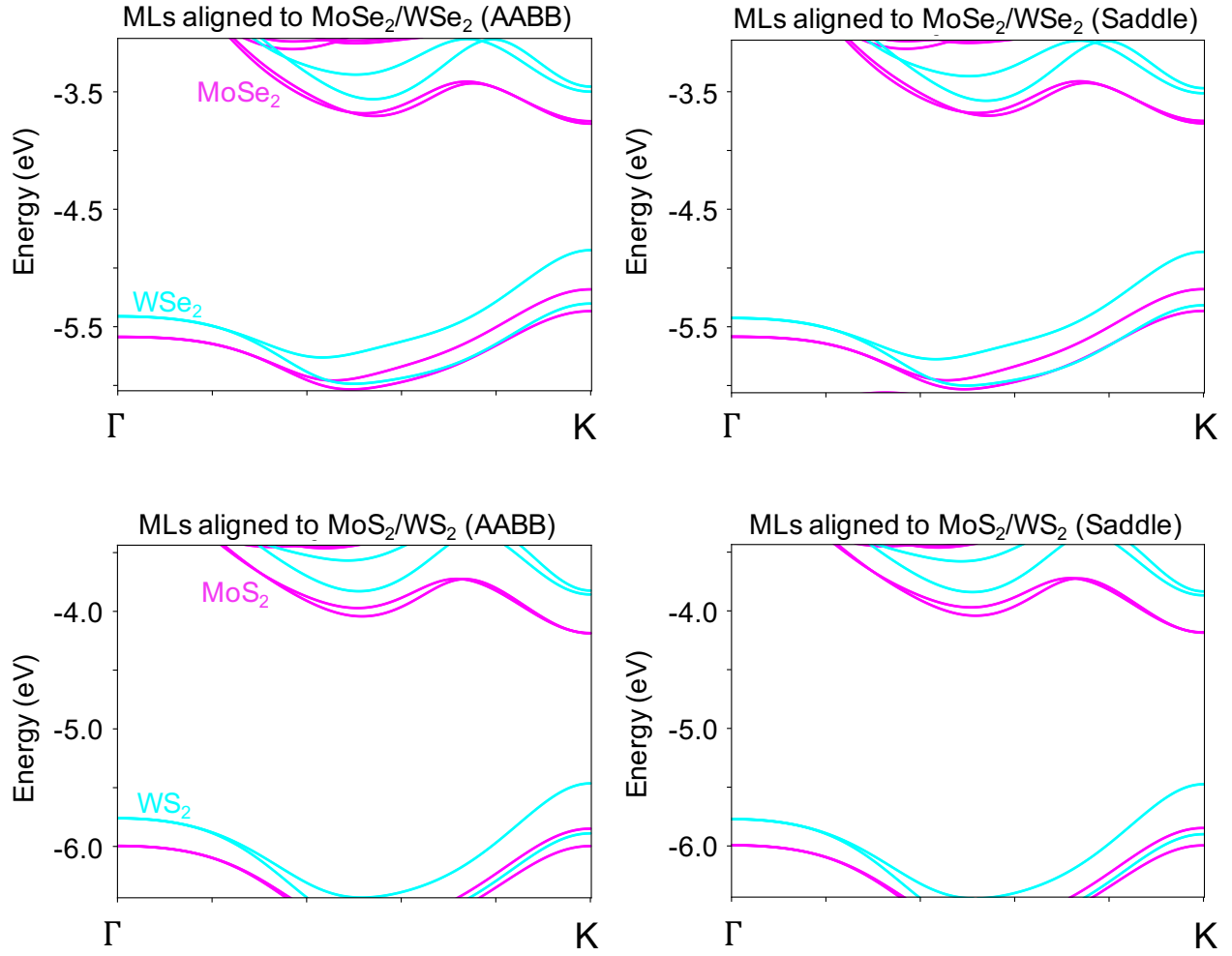


FIG. S4: Aligned monolayer bands for the higher energy structures in the 0° stacking space. The conduction band edge of each monolayer at K is aligned with the appropriate bilayer pure state at K. (i.e. The MoX_2 conduction band edge is aligned with the bilayer conduction band minimum, which is entirely localized in the MoX_2 layer, and the WX_2 conduction band edge is aligned with the third lowest bilayer conduction band at K, which is entirely localized on the WX_2 layer.) Magenta bands are the MoX_2 bands and cyan bands are the WX_2 bands.

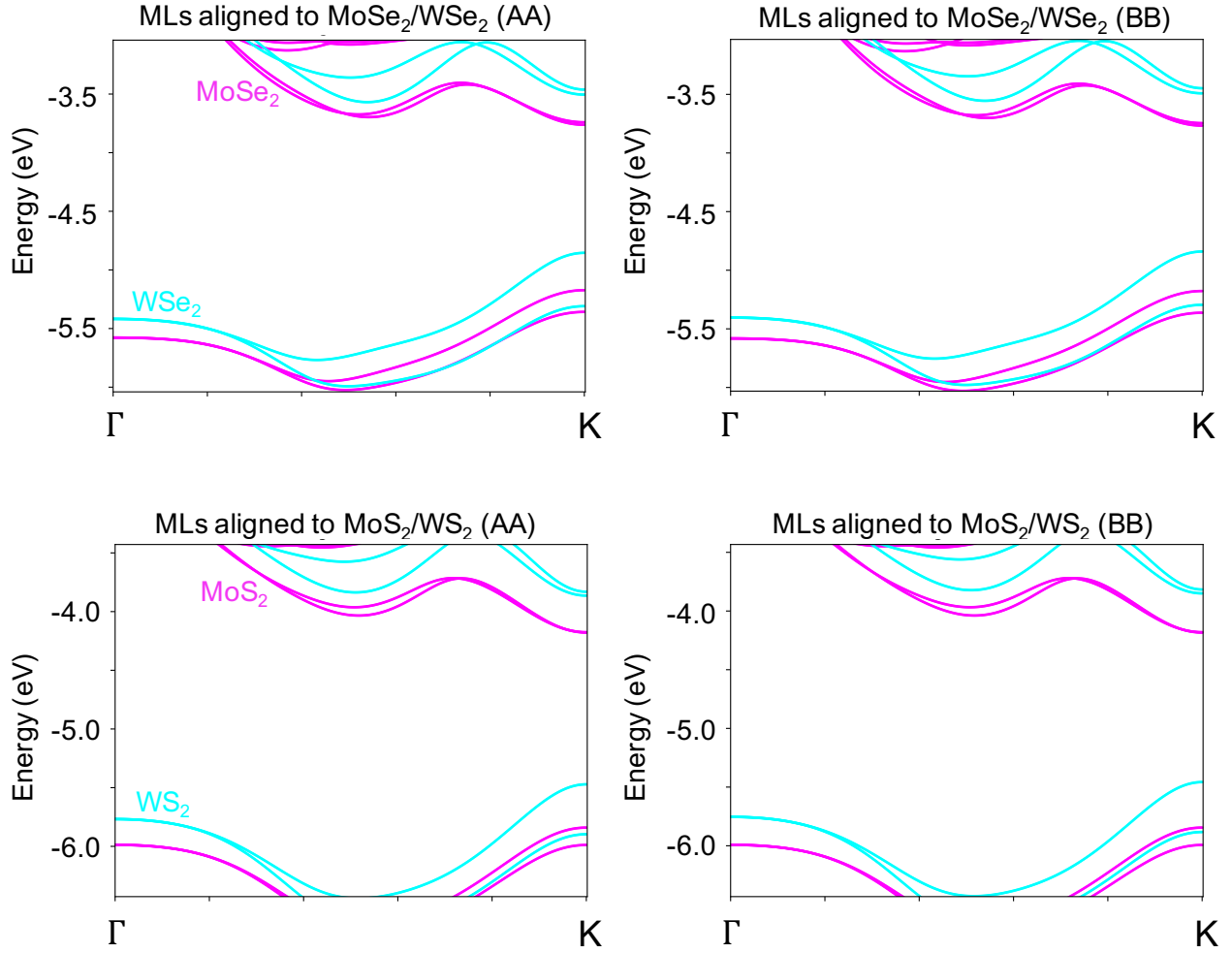


FIG. S5: Aligned monolayer bands for the higher energy structures in the 60° stacking space. The conduction band edge of each monolayer at K is aligned with the appropriate bilayer pure state at K. (i.e. The MoX₂ conduction band edge is aligned with the bilayer conduction band minimum, which is entirely localized in the MoX₂ layer, and the WX₂ conduction band edge is aligned with the third lowest bilayer conduction band at K, which is entirely localized on the WX₂ layer.) Magenta bands are the MoX₂ bands and cyan bands are the WX₂ bands.

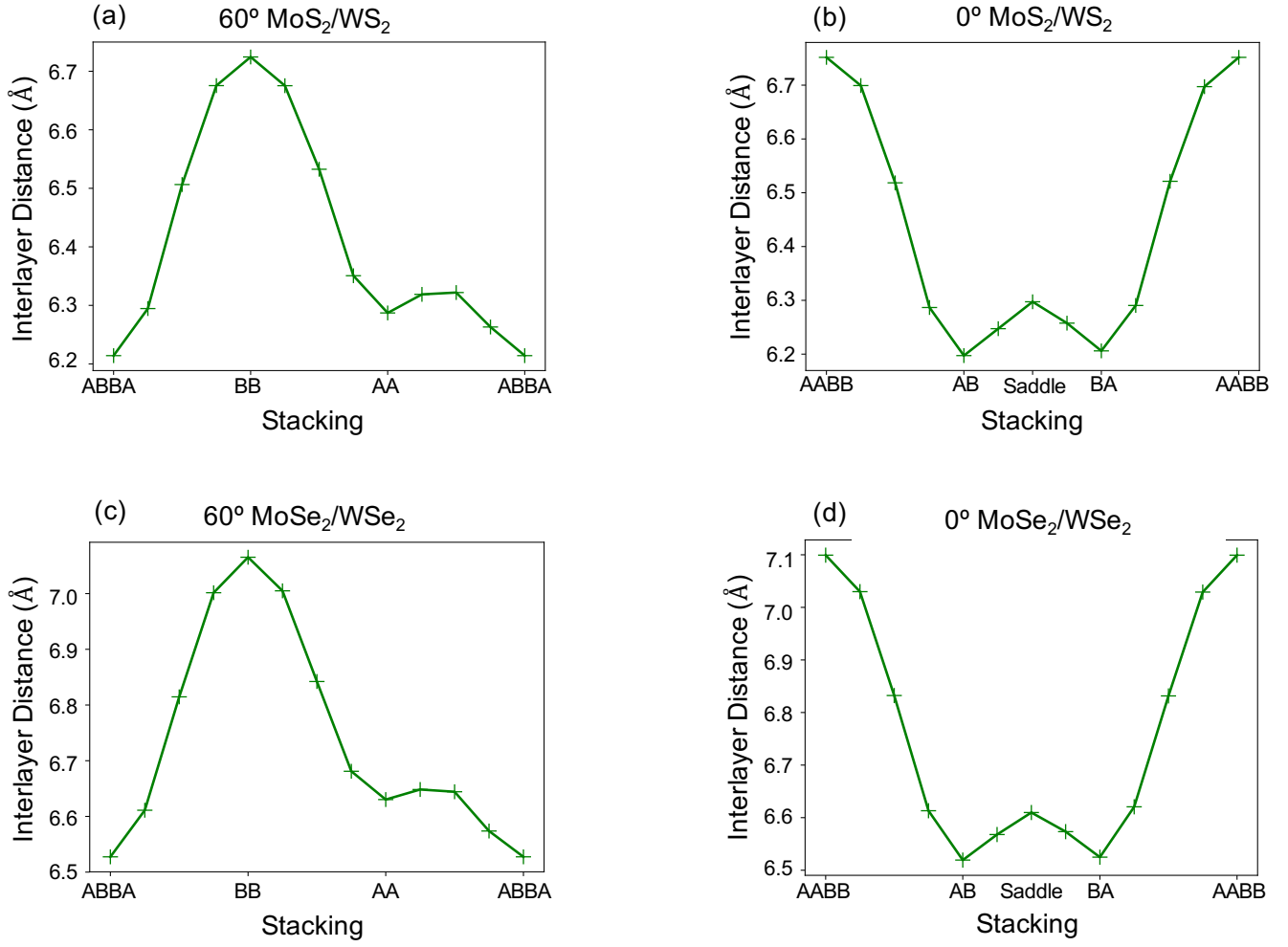


FIG. S6: Interlayer distances plotted with respect to stacking geometries for (a) 60° and (b) 0°-aligned MoS₂/WS₂ bilayers and (c) 60° and (d) 0°-aligned MoSe₂/WSe₂ bilayers. Interlayer distance is measured between the metal atoms of the two layers. The difference in interlayer distance between the degenerate ground states (AB and BA) in 0°-oriented MoS₂/WS₂ is 0.009 Å, while the difference in interlayer distance between the degenerate ground states (AB and BA) in 0°-oriented MoSe₂/WSe₂ is 0.006 Å.